



Trans. Nonferrous Met. Soc. China 27(2017) 2063-2072

Transactions of Nonferrous Metals Society of China

www.tnmsc.cn



Redox behavior and chemical species of arsenic in acidic aqueous system

Jin-qin YANG¹, Li-yuan CHAI^{1,2}, Qing-zhu LI^{1,2}, Yu-de SHU^{1,2}

- 1. School of Metallurgy and Environment, Central South University, Changsha 410083, China;
- 2. National Engineering Research Centre for Control and Treatment of Heavy Metal Pollution, Central South University, Changsha 410083, China

Received 16 September 2016; accepted 20 January 2017

Abstract: Arsenic (As) removal from smelting acidic wastewater is an urgent task. The most common method is oxidation of trivalent As(III) to pentavalent As(V) subsequently precipitated by ferric (Fe(III)) salts. Foundations of redox behavior and chemical species are of great importance for understanding As removal. In this work, cyclic voltammetry (CV) and UV–Vis spectroscopy were used for laboratory observation; meanwhile HSC and MINTEQ software were employed for theoretical analyses. It is found that As(III) oxidation, a multiple electron transfer reaction, is diffusion-controlled. The oxidation over-potential is very high (about 0.9 V) in sulfuric acid solutions (pH 1.0). In addition, Fe(III)–As(V) complexes are evidenced by UV–Vis spectra and chemical species analyses in series of Fe(III)–As(V)–H₂SO₄–H₂O solutions. Therefore, the Fe(III) and As(V) species distribution against pH values are determined and a new φ –pH diagram with inclusion of Fe–As complexes is consequently compiled based on thermodynamic data predicted by other researchers.

Key words: arsenic; ferric-arsenic complexes; φ -pH diagram; chemical species; acidic wastewater

1 Introduction

Arsenic (As) is often found in association with nonferrous metal ore [1]. In nonferrous metal smelters, As-containing acidic wastewater was generated from the wet scrubber process of smelting fume [2]. The smelting acidic wastewaters sampled from certain copper smelter and lead-zinc smelter (see Table 1) are very different from common wastewaters, i.e., groundwater, and municipal wastewater [3]. The extremely low pH value, abundant As and complicated composition lead to difficulty in As removal.

One of the potential sources of As is the As_2O_3 -bearing flue dust generated by smelting operations [4,5]. Thus, trivalent state As(III) is predominant, e.g., the ratio of As(III)/As(total) is equal to 67% and 85% in lead–zinc and copper smelting acidic wastewaters, respectively (Table 1). A pre-oxidation treatment is significant because As(III) is more mobile and toxic than pentavalent state As(V) [6]. The oxidation of As(III) to As(V) is unlikely to be a problem for the pressure oxidation systems but difficult under atmosphere [7].

Moreover, the on-site oxidation under strong acidic conditions is challenging. Lime neutralization is commonly used for acidic wastewater treatment. However, lime can produce plenty of gypsum and unstable cadmium arsenate [8]. Consequently, the on-site high-effective oxidation is attractive, which can lay foundation for the subsequent ferric arsenate (FeAsO₄) precipitation under strong acidic conditions. As coprecipitation with ferric (Fe(III)) iron has been specified by U.S. EPA as the best demonstrated available technology (BDAT) for the removal of As [9]. Scorodite (FeAsO₄·2H₂O), ferric arsenate and arsenical ferrihydrite are common precipitates formed from As removal in metallurgical industries [10]. Well-crystalline scorodite is more advantageous in lower ferric demand, higher density and greater stability. The production of scorodite is easily conducted under autoclave conditions, i.e., under high temperature and pressure conditions [11].

However, atmospheric scorodite production is of great concern due to lower capital investment [8]. Works done over last decades by DEMOPOULOS and coworkers [5,12,13] achieved the production of scorodite by step-wise lime neutralization at 90 °C. In addition,

Table 1 Compositions of acidic wastewaters from different smelters (mg/L)

Component	#1	#2
S	8182	26435
As(total)	2335.5	9010
As(III)	1557	7660
Na	14371	7038
Ni	0.55	735.6
Si	373.7	674.8
Ca	23.05	537.3
Zn	2.6	369
Bi	_	256.1
Cu	0.85	184.1
Fe	4896.5	124.9
Mg	2.5	108.9
K	15.4	72.5
Cd	12.25	42.8
Al	16.65	27.8
Pb	4.15	4.2
Co	0.25	2.4
P	27.7	1.8
Mn	5.55	1.3
Hg	0.45	0.05

#1: Lead-zinc smelting acidic wastewater (pH=1.88); #2: Copper smelting acidic wastewater (pH=1.21); Trivalent As(III) was determined by HG-AFS and other pollutants by ICP-AES.

scorodite was precipitated from sulfuric acid at pH 2 at temperatures as low as 70 °C, but the long reaction time of 16 h was needed [13]. This is because amorphous ferric arsenate is the initial precipitate, which was formed almost immediately and then transformed into scorodite [14]. Previously, it was found that aqueous Fe(III)-As(V) complexes can convert into colloid ferric arsenate under higher temperature and pH conditions [15]. The conversion of aqueous complexes to amorphous ferric arsenate and subsequently to scorodite is meaningful for the removal of As(V) from acidic effluents by coprecipitation with Fe(III). Therefore, thermodynamic chemistry is needed to be studied to provide an insight into the species distribution and transformation in acidic Fe-As system.

In this work, the redox of As in acidic solutions was studied by the combination of cyclic voltammetry (CV) method and theoretical φ -pH diagram analysis. In addition, the species of As in As-H₂O and As-Fe-H₂SO₄-H₂O systems were discussed. The new φ -pH diagram for As-Fe-H₂SO₄-H₂O system was constructed with the inclusion of aqueous Fe(III)/Fe(II)-As(V) complexes.

2 Calculation and experiment methods

2.1 Calculation methods

The φ -pH diagram was constructed based on the well-known Nernst equation. A half-cell reaction can be written as follows:

$$cA+dD+ne = xX+yY$$
 (1)

The corresponding Nernst equation was written as Eq. (2). Reversible potential (φ^0) can be derived from the Gibbs free energy of reaction as Eq. (3):

$$\varphi = \varphi^0 + \frac{RT}{nF} \ln \frac{a_X^x a_Y^y}{a_A^a a_D^d}$$
 (2)

$$\varphi^0 = -\frac{\Delta G_{\rm f}^0}{nF} \tag{3}$$

where *a* represents the activity of substances; *F* is the Faraday's constant. Software HSC 7.1 was used in this work for the construction of φ -pH diagrams. If not specified, the Gibbs free energies in database of HSC 7.1 were adopted.

Visual MINTEQ 3.1 was used to determinate the speciation–pH diagram. The calculation processes were illustrated by taking As(V) (H_x AsO₄^{x-3}) as an example. The formation reaction and corresponding constant equation was shown as Eqs. (4)–(6), where square brackets represent concentration. The sum of H_x AsO₄^{x-3} is equal to the total concentration of As(V) (Eq. (7)). The fractions of As(V) species at various pH values were then solved by MINTEQ 3.1.

$$H^{+} + AsO_{4}^{3-} \rightarrow HAsO_{4}^{2-}, K_{a}^{0} = \frac{[HAsO_{4}^{2-}]}{[AsO_{4}^{3-}][H^{+}]}$$
 (4)

$$H^{+} + HAsO_{4}^{2-} \rightarrow H_{2}AsO_{4}^{-}, K_{a2}^{0} = \frac{[H_{2}AsO_{4}^{-}]}{[HAsO_{4}^{2-}][H^{+}]}$$
 (5)

$$H^{+} + H_{2}AsO_{4}^{-} \rightarrow H_{3}AsO_{4}, K_{a3}^{0} = \frac{[H_{3}AsO_{4}]}{[H_{2}AsO_{4}^{-}][H^{+}]}$$
 (6)

$$[As(V)] = [H_3AsO_4] + [H_2AsO_4^-] + [HAsO_4^{2-}] + [AsO_4^{3-}]$$
(7)

Same method was used for the determination of As(III) and Fe(III) species distribution against pH value. If not specified, the formation constants in database of MINTEQ 3.1 were adopted. However, the species distribution against pH can be affected by ionic strength (IS). The equilibrium constant at a given ionic strength (K_n^I) is given by the activity coefficients of the species involved in the equilibrium (Eq. (7)):

$$K_n^I = K_n^0 \times \frac{\gamma_{H_x A s O_n^{x-3}}}{\gamma_{H^+} \times \gamma_{H_{x-1} A s O_n^{x-4}}}$$
(8)

In MINTEQ software, IS is calculated based on Eq. (9). The activity coefficient at I < 0.3 mol/L is calculated from the Davies equation as Eq. (10):

$$I = 0.5 \sum m_i \cdot z_i^2 \tag{9}$$

$$-\lg \gamma_i = A \cdot z_i^2 \left(\frac{\sqrt{I}}{1 + \sqrt{I}} - B \cdot I \right)$$
 (10)

where γ_i is the activity coefficient of species i, I is the ionic strength, z_i is the charge of the species, A is the Debye–Hückel coefficient, which takes the value of 0.51 at 25 °C, and B is the so-called Davies B parameter, which has a default value of 0.3.

2.2 Experimental methods

1) Cyclic voltammetry (CV) experiments

For the preparation of experimental solutions, pH 1.0 sulfuric acid was prepared in advance as supporting electrolyte. As(III) was incorporated into solutions by NaAsO₂ (Shanghai No. 4 Chemical Reagent Factory, China). Solutions referred to as "blank" contained no As. Cyclic voltammetry (CV) experiments were carried out by a three-electrode test system with a gold working electrode, glassy-carbon counter electrode and saturated calomel reference electrode. The solution was placed in a five-necked electrolysis pool in 25 °C water bath. High purity nitrogen gas was purged into the solutions before applying the potential.

2) UV-Vis spectroscopic experiments

Dilute sulfuric acid solution (50 mmol/L) was prepared using ultrapure water beforehand and used to prepare stock solutions and sample solutions in order to avoid the hydrolysis of Fe(III). The Fe(III) stock solution and As(V) stock solution were prepared by using Fe₂(SO₄)₃ (Xilong, Guangdong Province, China) and $Na_3AsO_4 \cdot 12H_2O$ (Sinopharm, Shanghai, respectively. A series of sample solutions containing 0.5 mmol/L Fe(III) and 0-55 mmol/L As(V) were prepared for UV-Vis tests (Table 2). UV-Vis spectroscopic measurements were performed using a Shimadzu (Japan) UV-2550 double-beam spectrophotometer. A baseline correction was carried out by filling in quartz cells of 1 cm light length with ultrapure water. The spectra were recorded by replacing the ultrapure water with sample solutions in sample cell.

3 Results and discussion

3.1 Redox behavior of As

The φ -pH diagram for As-H₂O system was reported in a number of works [16–20], but the stoichiometry of As(III) species was different. HAsO₂ stoichiometry was supported by the mass spectrometry, because mass-to-charge ratios (m/z) of 107 corresponding to AsO₂⁻ ion in the gas phase [21]. However, H₃AsO₃, a moiety comprising one As atom coordinated by three OH ligands, was supported by Raman and EXAFS spectroscopy [22–24]. Thus,

Table 2 Solution composition used in UV-Vis experiment and related calculation results

No.	$[H_2SO_4]_t/(mmol \cdot L^{-1})$	$[Fe_2(SO_4)_3]_t/(mmol \cdot L^{-1})$	$[Na_3AsO_4]_t/(mmol \cdot L^{-1})$	pH^1	pH^2	IS^2	pH^3	IS ³
1			0	1.35	1.293	0.0791	1.293	0.0791
2			0.5	1.36	1.301	0.0796	1.302	0.0796
3			1	1.41	1.310	0.0800	1.310	0.0800
4			2	1.42	1.327	0.0810	1.328	0.0809
5			4	1.43	1.363	0.0831	1.366	0.0829
6			6	1.44	1.400	0.0853	1.405	0.0850
7			8	1.48	1.440	0.0878	1.448	0.0874
8			10	1.52	1.482	0.0904	1.494	0.0899
9	50	0.25	15	1.63	1.597	0.0980	1.624	0.0971
10			20	1.76	1.730	0.1071	1.786	0.1059
11			25	1.92	1.881	0.1176	1.997	0.1162
12			30	2.10	2.056	0.1292	2.296	0.1281
13			35	2.44	2.261	0.1416	2.714	0.1410
14			40	2.83	2.517	0.1546	3.164	0.1543
15			45	3.75	2.893	0.1678	3.646	0.1678
16			50	6.00	4.123	0.1818	4.730	0.1820
17			55	6.36	5.870	0.2042	5.905	0.2048

^{1:} Measured results; 2: Calculation results with exclusion of Fe(III)-As(V) complexes; 3: Calculation results with inclusion of Fe(III)-As(V) complexes

 ${
m H_3AsO_3}$ and its conjugate base were considered here rather than HAsO₂. As given in Table 3, the Gibbs free energies of As(III) and As(V) species in HSC 7.0 database are in accordance with those in most reports. Consequently, the φ -pH diagram for As (0.1 mol/L)-H₂O system was directly constructed by using HSC 7.0 software.

As depicted in Fig. 1, the predominance fields for As(V) species under oxidizing conditions are similar to all published φ -pH diagrams. The field boundary for As(III) species was different because of the inclusion of $HAsO_3^{2-}$ and AsO_3^{3-} . Moreover, the critical potentials of As(V)/As(III) couples drop with decreasing pH value, which indicates that the oxidation of As(III) to As(V) is more feasible in alkaline than in acidic solutions. Thus, the redox behavior of As(III) under strong acidic wastewater is challenging. The practice redox behavior of As(III) in sulfuric acid (pH=1.0) was studied by cyclic voltammetry (CV) methods. Figure 2 shows that the voltammogram of a solution contains 0.1 mol/L As(III) and a blank solution. There are six peaks on the CV curve in 0.1 mol/L As(III) solution (blue line). The peaks B and C correspond to the oxygen evolution and the reduction of the oxide layer in comparison with the CV curve in blank solution (red line). The other four peaks A, D, E and F may be related to the redox behavior of As(III). To verify this, a series of CV tests were conducted in As(III)-bearing solutions with different concentrations.

As shown in Fig. 3, the locations of peaks A, D and F all shift to high potential as the concentration of As(III) increases. Moreover, the currents of peak A, D and F increase with As(III) concentration increasing. Peak A obviously splits into three small peaks when As(III) concentration is less than 5 mmol/L. Thus, peak A corresponds to a multiple electron transfer process. Figure 3(b) shows that the current of first electron transfer reaction is linearly correlated with As(III) concentration (R^2 =0.9985). Peak A is identified as the oxidation of As(III) to As(V). However, the oxidation over-potential of 0.1 mol/L As(III) in sulfuric acid

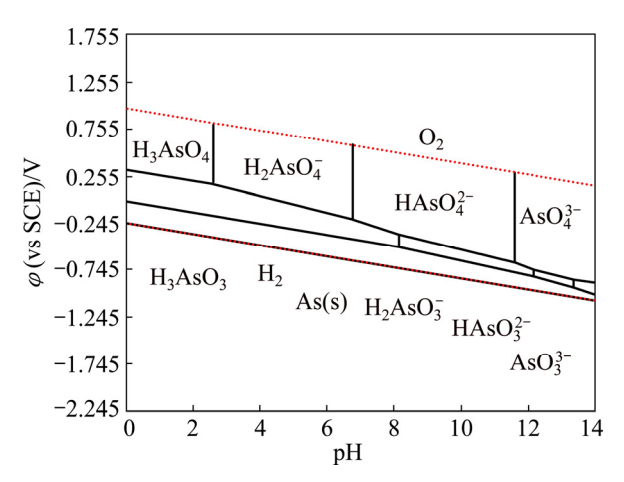


Fig. 1 φ (vs SCE)-pH diagram in As (0.1 mol/L)-H₂O system at 25 °C and 10⁵ Pa

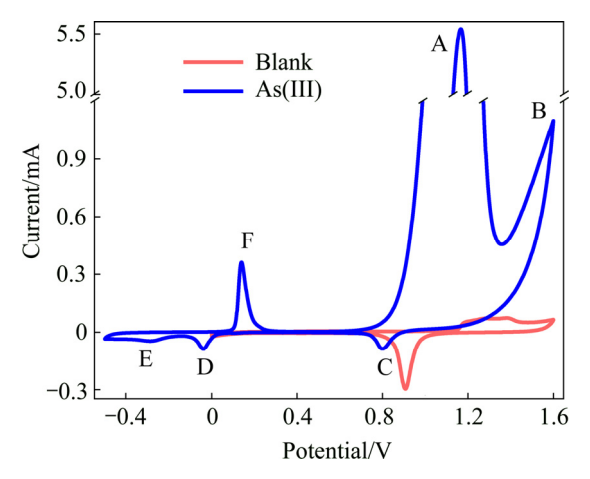


Fig. 2 Voltammogram in 0.1 mol/L As(III) solution (blue line) and blank solution (red line) (ν =50 mV/s)

solutions (pH 1.0) is about 0.9 V over the theoretical potential (about 0.3 V derived from Fig. 1). Peak D corresponds to the reduction of As(III), because peak current is linearly correlated to As(III) concentration. However, as shown in Fig. 3(c), the slope of fitting line is different in As(III) ranges of 0–1, 1–2 and 2–5 mmol/L. This indicates that multilayer As(s) is electrodeposited from As(III) on gold electrode. As for

Table 3 Gibbs free energies of $H_x AsO_3^{x-3}$ and $H_x AsO_4^{x-3}$ (kJ/mol)

Species	This work	Ref. [25]	Ref. [26]	Ref. [27,28]	Ref. [29]	Ref. [30]	Ref. [31]
$AsO_3^{3-}(a)$	-4s46.99	-	_	-447.69	-	_	-
$AsO_4^{3-}(a)$	-647.58	-647.9	-651.87	-647.9	_	-648.39	-648.52
$H_3AsO_3(a)$	-638.98	-639.29	-646.01	-639.29	-639.90	-639.85	-639.80
$H_3AsO_4(a)$	-767.32	-765.36	-769.86	-765.36	-766.10	-766.09	-766.09
$HAsO_3^{2-}(a)$	-523.20	-	-524.26	-524.26	-	-	-507.40
$HAsO_4^{2-}(a)$	-713.74	-714.03	-717.56	-714.03	-714.70	-714.59	-713.73
$H_2AsO_3^-(a)$	-592.54	-586.66	-593.29	-586.66	_	-587.14	-587.66
$H_2AsO_4^-(a)$	-752.35	-752.57	-757.56	-752.57	_	-753.16	-753.12

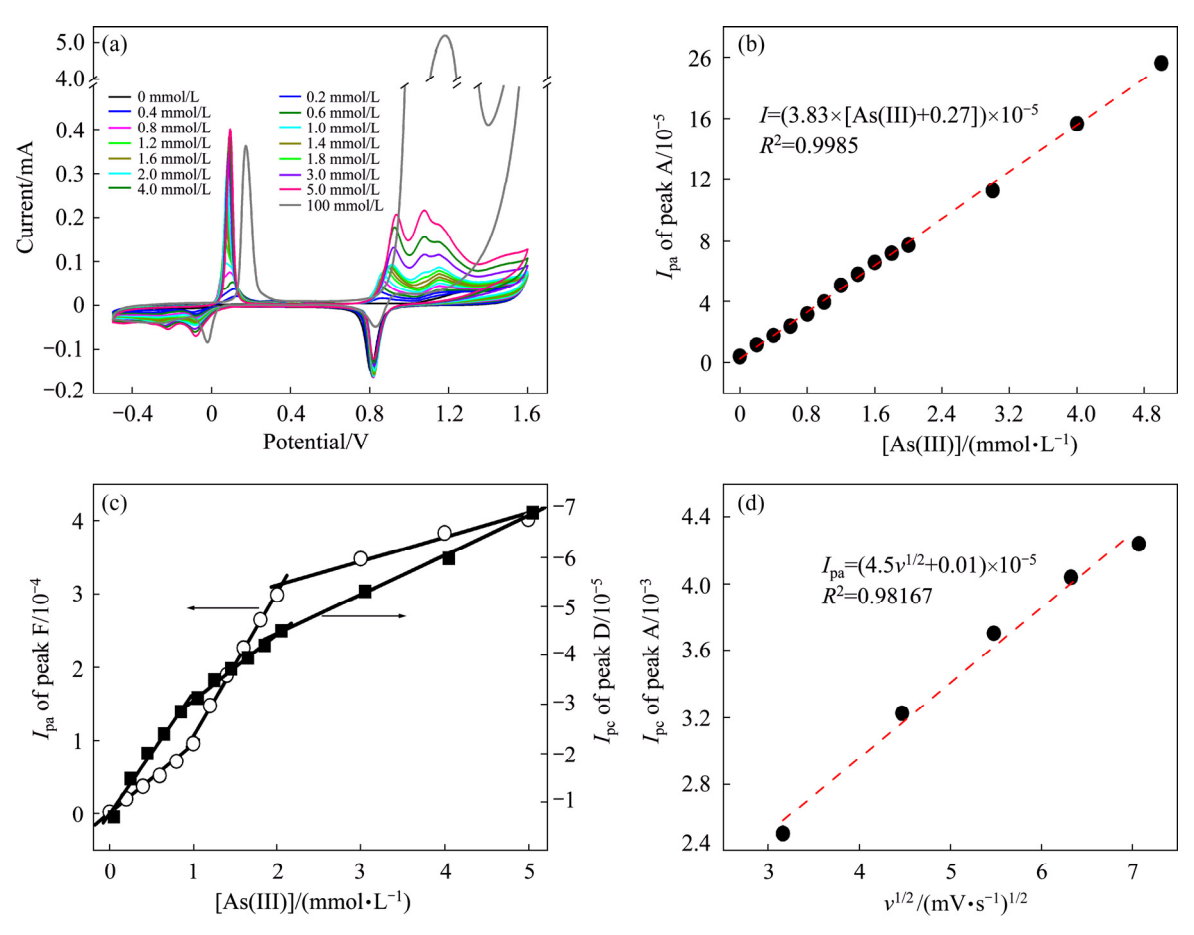


Fig. 3 Voltammograms in As(III) solutions (a), linear calibration plots of peak current against As(III) concentration ([As(III)]= 0–5 mmol/L, v=50 mV/s) (b) and (c), and linear calibration plots of peak A current against $v^{1/2}$ ([As(III)]=0.1 mol/L, v=10, 20, 30, 40, 50 mV/s) (d)

the weak peak E, it can be explained as outmost As(s) electrodeposited from As(III) or from As(V). The reduction of As(V) to As(s) is thermodynamic sluggish, but the electrogenerated H₂ could chemically reduce As(V) to As(s) [32]. Following peak D and E, the peak F is no doubt the oxidation of As(s) to As(III). Thus, the linear correlation between peak current and As(III) concentration is in accordance with that of peak D. As shown in Fig. 3(c), three lines with different slopes are suitable for fitting in the As(III) concentration ranges of 0-1, 1-2 and 2-5 mmol/L. The consistent trend between peak D and F confirms that As(s) is layeredly electrodeposited on Au electrode. In addition, the oxidation process of As(III) to As(V) was investigated at different scan rates. The good linear relationship between peak current and scan rate $(v^{1/2})$ (Fig. 3(d)) indicates that As(III) oxidation is mainly diffusion-controlled.

3.2 Chemical species of As

As(III) and As(V) mainly exist as $H_x AsO_3^{x-3}$ and $H_x AsO_4^{x-3}$ ($0 \le x \le 3$) in As- $H_2 O$ system, respectively. The speciation-pH diagrams for As(III) and As(V) were calculated at ionic strength of 0 based on thermodynamic

reported by MARINI and formation constants ACCORNERO [33]. The thermodynamic constants (K_n^0) for As(III) and As(V) species are reviewed in Table 4. As given in Table 4, there is no significant difference among different reports. As depicted in Fig. 4(a), As(V) predominantly exists as (1) H₃AsO₄ and $\rm H_2AsO_4^-$ at pH 0-4.5, (2) $\rm H_2AsO_4^-$ and $\rm HAsO_4^{2-}$ at pH 4.5-9, and (3) $\rm HAsO_4^{2-}$ and $\rm AsO_4^{3-}$ at pH 9-14. The major form of As(V) is neutral molecules H₃AsO₄ at pH<2, thus it is hard to be removed by electrostatic adsorption. Figure 4(b) shows that As(III) mainly exists as (1) H_3AsO_3 at pH=0-7.5, (2) H_3AsO_3 and $H_2AsO_3^$ at pH=7.5-10.5, (3) $H_2AsO_3^-$ and $HAsO_3^{2-}$ at pH= 10.5-12 and (4) $H_2AsO_3^-$, $HAsO_3^{2-}$ and AsO_3^{3-} at pH=12-14. Accordingly, H₃AsO₃ is the only As(III) species under acidic solutions. It is reported that undissociated H₃AsO₃ does not react with H₂O₂ [34] However, rate constant k for the oxidation reaction between As(III) and H₂O₂ can be determined by pH, temperature and IS at pH=7.5-10.3 [34]. This is mainly because the molar fraction of $H_2AsO_3^-$, $HAsO_3^{2-}$ and AsO_3^{3-} species can be affected by pH, temperature and

<u> </u>	A	J 1	т			
Reaction	Ref. [27]	Ref. [26]	Ref. [29]	Ref. [35]	Ref. [31]	Ref. [33]
$H^+ + H_2 AsO_4^- \rightarrow H_3 AsO_4$	2.24	2.2	2.2	2.2	2.2	2.20
$\text{H}^+\text{+}\text{HAsO}_4^{2-}\to\text{H}_2\text{AsO}_4^-$	6.96	6.96	6.96	6.9	7.08	6.97
$\text{H}^+ + \text{AsO}_4^{3-} \rightarrow \text{HAsO}_4^{2-}$	11.5	11.5	11.5	11.5	11.5	11.53
$H^+ + H_2 AsO_3^- \rightarrow H_3 AsO_3$	9.2	9.22	9.2	9.2	9.22	9.22
$H^++HAsO_3^{2-} \rightarrow H_2AsO_3^-$	12.1	12.10	12.1	12.1	12.3	12.13
$H^+ + AsO_3^{3-} \rightarrow HAsO_3^{2-}$	13.4	13.41	_	13.4	_	13.4

Table 4 Thermodynamic formation constants of $H_x AsO_3^{x-3}$ and $H_x AsO_4^{x-3}$ ($0 \le x \le 3$)

Data in table are $\lg K_n^0$ rather than K_n^0

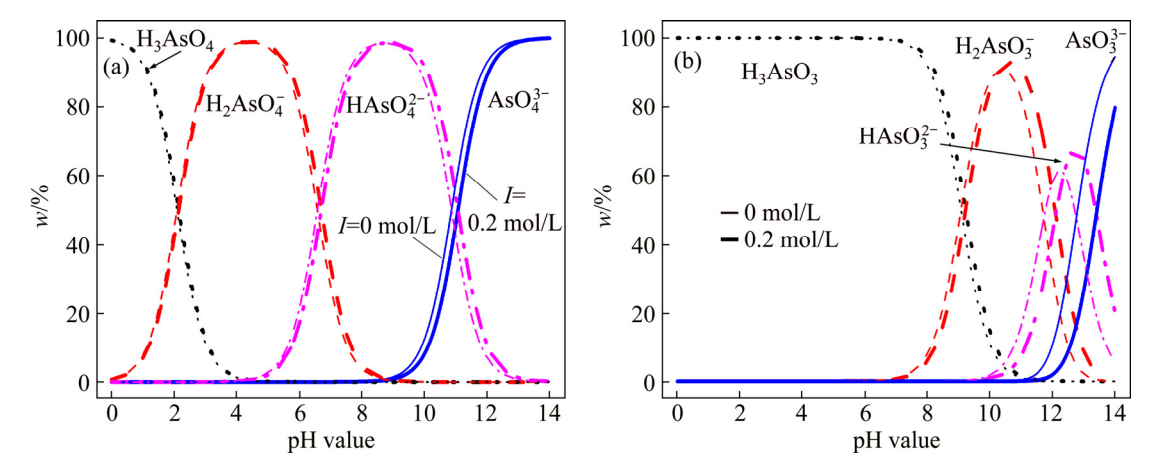


Fig. 4 Speciation-pH diagrams of As(V) species (a) and As(III) species (b) in As-H₂O system at 25 °C

IS. The speciation—pH diagram at *I*=0.2 mol/L was determined based on the Davies equation (Eq. (8)). As depicted in Fig. 4, high IS facilitates deprotonation reaction. Therefore, negatively-charged species with higher fraction under high IS solutions can be absorbed on the positive-charged surfaces.

In addition, it is predicted that As(V) can complex with metal ion to form aqueous complexes [33]. Fe(III) is usually used as precipitator, thus the complexation between As(V) and Fe(III) is studied here by UV-Vis spectroscopy. The experimental solutions prepared by Fe₂(SO₄)₃, H₂SO₄ and Na₃AsO₄ are all acidic solutions. Figure 5 shows that a new peak at about 240-300 nm appears as As(V) concentration increases. The new peak is attributed to Fe(III)-As(V) complexes. The pH value, IS and the fraction of various Fe(III) species were calculated by MINTEQ 3.1 with the consideration of Fe(III)-As(V) complexes or not. The lgK reported by MARINI and ACCORNERO [36] were adopted here, because they are in accordance with other reports excluding that of FeAsO₄(a) (see Table 5). As displayed in Table 2, the calculated pH values are lower than measured ones, but slightly higher when Fe(III)-As(V) complexes are considered.

The Fe(III) species in experimental solutions are shown in Fig. 6. Figure 6(a) shows that Fe(III) predominantly exists as FeSO₄⁺ when As(V)

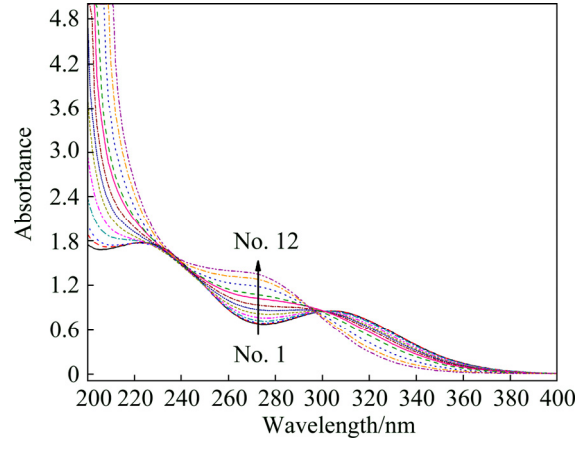


Fig. 5 UV–Vis spectra of $Fe_2(SO_4)_3$ – Na_3AsO_4 – H_2SO_4 – H_2O solutions

concentration is less than 45 mmol/L and as Fe(OH)⁺₂ when As(V) concentration is 45–50 mmol/L. It was reported that the band maxima of Fe(OH)⁺₂ occur at the wavelength of 300 nm [40]. The new peak at 240–300 nm is indeed not due to Fe(OH)⁺₂. When Fe(III)–As(V) complexes were considered in the calculations (Fig. 6(b)), FeH₂AsO²⁺₄ and FeHAsO⁺₄ become the major species in solutions with 15–40 mmol/L As(V) and FeHAsO⁺₄ is almost the only soluble Fe(III) species when As(V) concentration is 40–50 mmol/L. In addition, the saturation index is higher than 0.577 when [As(V)]

Complex -	$\Delta G/(\mathrm{kJ})$	$\Delta G/(\mathrm{kJ \cdot mol}^{-1})$		$\lg K(M^{n} + H_{3}AsO_{4} = MH_{m}AsO_{4}^{n+m-3}) + (3-m)H^{+})$					
	Ref. [37]	Ref. [36]	Ref. [38]	Ref. [39]	Ref. [37]	Ref. [33]	Ref. [36]		
Fe ^{III} H ₂ AsO ₄ ²⁺	-793.92	-793.97	1.8(1.74)	_	1.74	2.00(1.88)	2.07		
$Fe^{III}HAsO_4^+$	-787.24	-786.63	0.66(0.57)	_	0.57	0.71(0.59)	0.77		
$Fe^{III}AsO_4$	-771.49	-743.46	-1.8(-2.19)	_	-2.19	-6.86(-6.97)	-6.79		
$\mathrm{Fe^{II}H_{2}AsO_{4}^{+}}$	-860.42	-859.8	_	0.44(0.38)	0.38	0.53(0.41)	0.60		
$Fe^{II}HAsO_4$	-825.43	-823.30	_	-5.66(-5.75)	-5.75	-5.87(-5.99)	-5.81		
$Fe^{II}AsO_4^-$	-778.16	-780.27	_	-13.64(-14.03)	-14.03	-13.41(-13.53)	-13.35		

Table 5 Reaction equilibrium constants and Gibbs free energies of Fe-As(V) complexes

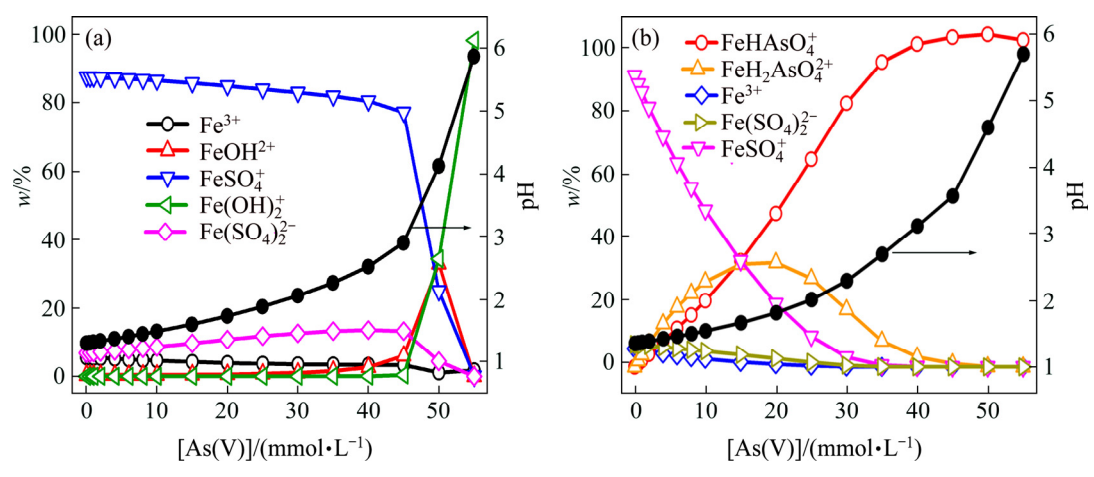


Fig. 6 Fe(III) species analyses in UV-Vis experiment solutions with exclusion (a) and inclusion (b) of Fe(III)-As(V) complexes

>30 mmol/L. Hematite, goethite, lepidocrocite and FeAsO₄·2H₂O etc are oversaturated, which can explain that experimental solutions become turbid when As(III) concentration is more than 30 mmol/L. Accordingly, Fe(III)-As(V) complexes are significant to be considered in Fe(III)- As(V)-H₂SO₄-H₂O solutions.

As discussed above, Fe(III)-As(V) complexes are important in the species analysis for the system of Fe(III)-As(V)-H₂SO₄-H₂O₇, a representative system of As(V) removal from acidic wastewater. Then, the speciation-pH diagrams of Fe(III) and As(V) were calculated for such a system with inclusion of Fe(III)-As(V) complexes. As displayed in Fig. 7(a), As(V) mainly exists as (1) $FeH_2AsO_4^{2+}$ and H_3AsO_4 at pH<1, (2) $FeH_2AsO_4^{2+}$, $FeHAsO_4^+$, H_3AsO_4 and $H_2AsO_4^-$ at pH=1-2, and (3) $H_2AsO_4^-$ at pH>2. As shown in Fig. 7(b), Fe(III) mainly exists as FeH₂AsO₄²⁺ at pH<2, and FeHAsO₄⁺ at pH>2. However, the total dissolved Fe(III) decreases when pH is higher than 2. Therefore, As(V) mainly exists as $FeH_2AsO_4^{2+}$, FeHAsO₄⁺, H₃AsO₄ and H₂AsO₄⁻ in acidic wastewater treatment system.

3.3 φ-pH diagram in Fe-As-H₂O system

As mentioned above, the Fe(III)-As(V) complexes are significant for the speciation of Fe(III) and As(V).

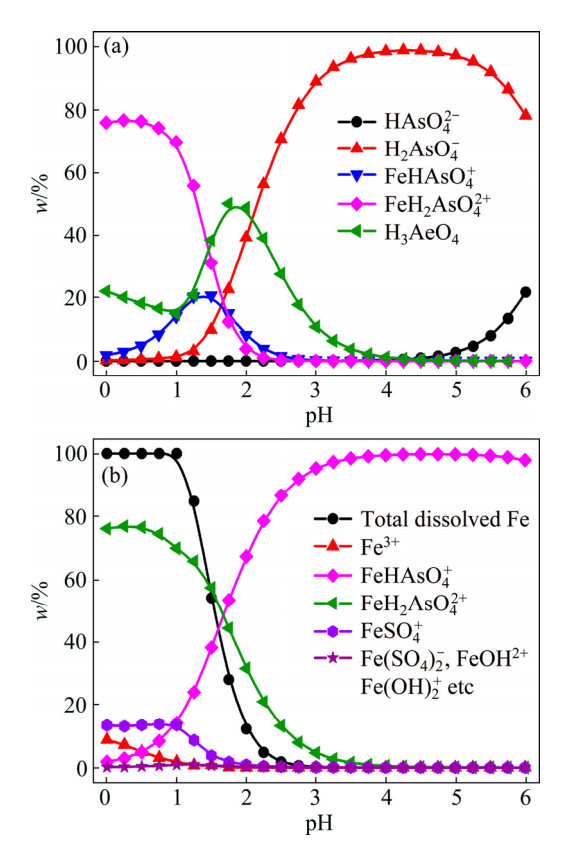


Fig. 7 Speciation-pH diagrams of As(V) (a) and Fe(III) (b) with inclusion of Fe(III)-As(V) complexes ([As(V)]=[Fe(III)]= $[SO_4]=0.1 \text{ mol/L})$

Fe(III)-As(V) complexes should be included in φ -pH diagram for As-Fe-H₂O system. According to literatures, Fe(III)-As(III), Fe(II)-As(V) and Fe(II)-As(III) complexes were predicted but there was no experimental evidence. Fe(III)-As(III) and Fe(II)-As(III) complexes are ruled out because of (1) the possible redox reaction between Fe(III) and As(III) and (2) the oxidation of As(III) in parallel to the dark oxidation of Fe(II) by dissolved O₂ [41]. Given the complexation ability of As(V), Fe(II)-As(V) complexes were considered here. Therefore, φ -pH diagram for Fe-As-H₂O system was constructed with inclusion of Fe(III)-As(V) and Fe(II)-As(V) complexes, and compared with one with exclusion of these complexes.

The φ -pH diagrams are depicted in Fig. 8 for As-Fe-H₂O system at 25 °C and 10⁵ Pa. Figure 8(a) with exclusion of Fe-As complexes shows that FeAsO₄(s) is predominant in the pH range of 1.2-3.4 under oxidizing conditions. It was reported that amorphous ferric arsenate could transform into scorodite [42]. The kinetics of scorodite formation and its transformation from ferric arsenic is strongly controlled by pH, for example, scorodite precipitated after ~384 h at pH 4.5 but ~13 at pH 1 [14]. The pH of

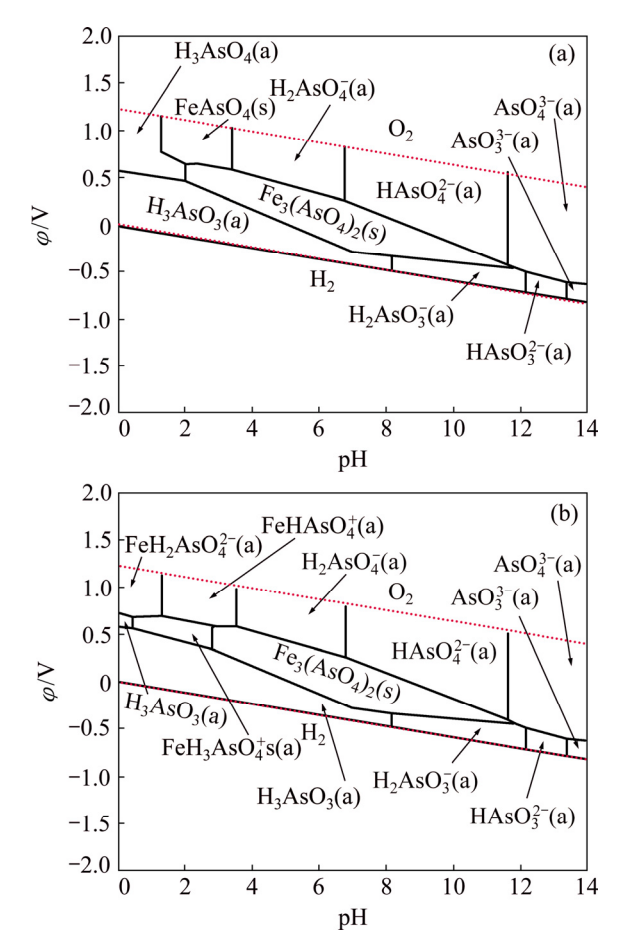


Fig. 8 φ -pH diagrams in 0.1 mol/L As-0.1 mol/L Fe-H₂O system with exclusion (a) and inclusion (b) of Fe-As complexes at 25 °C and 10⁵ Pa (φ = φ (vs SCE) + 0.245)

smelting acidic wastewater is usually less than 3, which is suitable for the production of ferric arsenate and scorodite. However, Fe(III)–As(V) complexes (FeH₂AsO₄²⁺, FeHAsO₄⁴ and FeH₂AsO₄⁴) were reported predominant under extremely acidic pH condition [43]. Therefore, the φ –pH diagram with inclusion of Fe–As complexes is more meaningful to understand the As geochemistry in Fe–As–H₂O system.

Fe-As complexes were not considered in previous *φ*–pH diagram mainly due to unreliability of thermodynamic data. Recently, MARINI ACCORNERO [36] estimated the equilibrium constants and Gibbs free energies, which are in good accordance with other reports [37–39]. Accordingly, a new φ -pH diagram for Fe-As-H₂O system was constructed based on the estimates. Figure 8(b) shows that Fe(III)-As(V) complexes shrink the stability field of H₃AsO₄ and FeAsO₄(s). Moreover, Fe(II)-As(V) complexes occur in pH range of 0.5-3. The predominant field of Fe₃(AsO₄)₂ is affected by Fe(II)-As(V) complexes. FeH₂AsO₄²⁺, FeHAsO₄⁺ and FeH₂AsO₄⁺ are all restricted at acidic pH conditions. Consequently, Fe-As(V) complexes are considerable in the As removal from smelting acidic wastewaters by coprecipitation with iron salts.

4 Conclusions

- 1) The cyclic voltammetry curves were tested in As(III)-containing sulfuric acid solutions (pH=1.0). It is shown that the over-potential of As(III) oxidation to As(V) is very high (about 0.9 V). Therefore, on-site peroxidation in acidic wastewater is challenging.
- 2) The UV–Vis spectra of a series $Fe_2(SO_4)_3$ – Na_3AsO_4 – H_2SO_4 – H_2O solutions show that a new peak at about 240–300 nm appears as As(V) concentration increases. Corresponding Fe(III) species analyses indicate that Fe(III)–As(V) complexes are formed in the experimental solutions.
- 3) The φ -pH diagram for Fe-As-H₂O system with inclusion of Fe-As(V) complexes were constructed and compared with the one with exclusion of Fe-As(V) complexes. The results illustrate that Fe(III)-As(V) complexes are stable under acidic conditions and shrink the stability field of H₃AsO₄ and FeAsO₄(s).

References

- [1] MANDAL B K, SUZUKI K T. Arsenic round the world: A review [J]. Talanta, 2002, 58(1): 201–235.
- [2] CHAI Li-yuan, YUE Men-qing, YANG Jin-qin, WANG Qing-wei, LI Qing-zhu, LIU Hui. Formation of tooeleite and the role of direct removal of As(III) from high-arsenic acid wastewater [J]. Journal of Hazardous Materials, 2016, 320: 620–627.
- [3] YANG W C, ZHAO N, ZHANG N, CHEN W, KAN A T, TOMSON M B. Time-dependent adsorption and resistant desorption of arsenic

- on magnetite nanoparticles: Kinetics and modeling [J]. Desalination and Water Treatment, 2012, 44:100–109.
- [4] CHAI Li-yuan, SHI Mei-qing, LIANG Yan-jie, TANG Jing-jie, LI Qing-zhu. Behavior, distribution and environmental influence of arsenic in a typical lead smelter [J]. Journal of Central South University, 2015, 22(4):1276–1286.
- [5] FILIPPOU D, DEMOPOULOS G P. Arsenic immobilization by controlled scorodite precipitation [J]. JOM, 1997,49(12): 52–55.
- [6] CHAI L Y, CHEN Y N, YANG Z H. Kinetics and thermodynamics of arsenate and arsenite biosorption by pretreated spent grains [J]. Water Environment Research A: Research Publication of the Water Environment Federation, 2009, 81(9): 843–848.
- [7] HARRIS B. The removal of arsenic from process solutions: Theory and industrial practice [J]. Hydrometallurgy, 2003, 2: 1889–1902.
- [8] FUJITA T, TAGUCHI R, ABUMIYA M, MATSUMOTO M, SHIBATA E, NAKAMURA T. Novel atmospheric scorodite synthesis by oxidation of ferrous sulfate solution. Part I [J]. Hydrometallurgy, 2008, 90(2): 92–102.
- [9] REDDY R G, RAMACHANDRAN V. Arsenic metallurgy [C]//TMS 2005 Annual Meeting. San Francisco, California, USA: Wiley, 2005.
- [10] MIN Xiao-bo, LIAO Ying-ping, CHAI Li-yuan, YANG Zhi-hui, XIONG Shan, LIU Lin, LI Qing-zhu. Removal and stabilization of arsenic from anode slime by forming crystal scorodite [J]. Transactions of Nonferrous Metals Society of China, 2015, 25(4): 1298–1306.
- [11] GONZALEZ-CONTRERAS P A. Bioscorodite: Biological crystallization of scorodite for arsenic removal [D]. Netherlands: Wageningen University, 2012.
- [12] SINGHANIA S, WANG Q, FILIPPOU D, DEMOPOULOS G P. Temperature and seeding effects on the precipitation of scorodite from sulfate solutions under atmospheric-pressure conditions [J]. Metallurgical and Materials Transactions B, 2005, 36(3): 327–333.
- [13] SINGHANIA S, WANG Q, FILIPPOU D, DEMOPOULOS G P. Acidity, valency and third-ion effects on the precipitation of scorodite from mixed sulfate solutions under atmospheric-pressure conditions [J]. Metallurgical and Materials Transactions B, 2006, 37(2): 189–197.
- [14] PAKTUNC D, DUTRIZAC J, GERTSMAN V. Synthesis and phase transformations involving scorodite, ferric arsenate and arsenical ferrihydrite: Implications for arsenic mobility [J]. Geochimica et Cosmochimica Acta, 2008, 72(11): 2649–2672.
- [15] YANG J, CHAI L, YUE M, LI Q. Complexation of arsenate with ferric ion in aqueous solutions [J]. RSC Advances, 2015, 5(126): 103936–103942.
- [16] LONG H. A fundamental study of the acidic pressure oxidation of orpiment and pyrite at high temperature [D]. British Columbia: University of British Columbia, 2000.
- [17] MASSCHELEYN P H, DELAUNE R D, PATRICK JR W H. Effect of redox potential and ph on arsenic speciation and solubility in a contaminated soil [J]. Environmental Science & Technology, 1991, 25(8): 1414–1419.
- [18] PIECZABA E, SANAK-RYDLEWSKA S, ZIĘBA D. Removal of arsenic from aqueous solutions by the method of precipitate flotation [J]. Archives of Mining Sciences, 2005, 50(1): 131–142.
- [19] YAZDI M R S, DARBAN A K. Effect of arsenic speciation on remediation of arsenic-contaminated soils and waters [C]//15th International Conference on Heavy Metals in the Environment (ICHMET). Gdansh, 2010: 492–495.
- [20] WU H. An empirical estimation of standard entropy for some complex cations and the E-pH diagram of As-H₂O system at elevated temperature [J]. Journal of Kunming University of Science and Technology, 1982, 3: 58-73.
- [21] DEBUSSCHERE L, DEMESMAY C, ROCCA J L. Arsenic speciation by coupling capillary zone electrophoresis with mass

- spectrometry [J]. Chromatographia, 2000, 51(5-6): 262-268.
- [22] GOUT R, POKROVSKI G, SCHOTT J, ZWICK A. Raman spectroscopic study of arsenic speciation in aqueous solutions up to 275 °C [J]. Journal of Raman Spectroscopy, 1997, 28(9): 725–730.
- [23] LOEHR T M, PLANE R A. Raman spectra and structures of arsenious acid and arsenites in aqueous solution [J]. Inorganic Chemistry, 1968, 7(9): 1708–1714.
- [24] MÄHLER J, PERSSON I, HERBERT R B. Hydration of arsenic oxyacid species [J]. Dalton Transactions, 2013, 42(5): 1364–1377.
- [25] ROSSINI F D, WAGMAN D D, EVANS W H, ROSSINI F D, ROSSINI F D. Selected values of chemical thermodynamic properties [M]. Washington, DC: US Government Printing Office, 1952.
- [26] SERGEYEVA E I, KHODAKOVSKIY I L. Physicochemical conditions of formation of native arsenic in hydrothermal deposits [J]. Geochemistry International, 1969: 846–859.
- [27] Technical Note 270-7. SCHUMM R H, WAGMAN D D, EVANS W H, PARKER V B. Selected values of chemical thermodynamic properties [S]. National Bureau of Standards, 1973.
- [28] WAGMAN D D, EVANS W H, PARKER V B, SCHUMM R H, HALOW I, BAILEY S M, CHURNEY K L, NUTTALL R L. Erratum: The NBS tables of chemical thermodynamic properties [J]. Journal of Physical and Chemical Reference Data, 1989,18(4): 1807–1812.
- [29] BARD A J, PARSONS R, JORDAN J. Standard potentials in aqueous solution [M]. New York: CRC Press, 1985.
- [30] SHOCK E L, HELGESON H C. Calculation of the thermodynamic and transport properties of aqueous species at high pressures and temperatures: Correlation algorithms for ionic species and equation of state predictions to 5 kb and 1000 °C [J]. Geochimica et Cosmochimica Acta, 1988, 52(8): 2009–2036.
- [31] NORDSTROM D K, ARCHER D G. Arsenic thermodynamic data and environmental geochemistry [M]//Arsenic in Ground Water. Boston, MA, USA: Springer, 2003: 1–25.
- [32] BU L, GU T, MA Y, CHEN C, TAN Y, XIE Q, YAO S. Enhanced cathodic preconcentration of As(0) at Au and Pt electrodes for anodic stripping voltammetry analysis of As(III) and As(V) [J]. The Journal of Physical Chemistry C, 2015, 119(21): 11400–11409.
- [33] MARINI L, ACCORNERO M. Prediction of the thermodynamic properties of metal–arsenate and metal–arsenite aqueous complexes to high temperatures and pressures and some geological consequences [J]. Environmental Geology, 2007, 52(7): 1343–1363.
- [34] PETTINE M, CAMPANELLA L, MILLERO F J. Arsenite oxidation by H_2O_2 in aqueous solutions [J]. Geochimica et Cosmochimica Acta, 1999, 63(18): 2727–2735.
- [35] VINK B W. Stability relations of antimony and arsenic compounds in the light of revised and extended E_h-pH diagrams [J]. Chemical Geology, 1996, 130(1): 21–30.
- [36] MARINI L, ACCORNERO M. Erratum to: Prediction of the thermodynamic properties of metal-arsenate and metal-arsenite aqueous complexes to high temperatures and pressures and some geological consequences [J]. Environmental Earth Sciences, 2010, 59(7): 1601–1606.
- [37] LANGMUIR D, MAHONEY J, ROWSON J. Solubility products of amorphous ferric arsenate and crystalline scorodite (FeAsO₄·2H₂O) and their application to arsenic behavior in buried mine tailings [J]. Geochimica et Cosmochimica Acta, 2006, 70(12): 2942–2956.
- [38] ROBINS R G. The stability and solubility of ferric arsenate: An update [EB/OL]. http://mdl.csa.com/partners/viewrecord.php. 1990.
- [39] WHITING K S. The thermodynamics and geochemistry of arsenic with application to subsurface waters at the sharon steel superfund site at Midvale, Utah [D]. Midvale: Colorado School of Mines, 1992.
- [40] KNIGHT R J, SYLVA R N. Spectrophotometric investigation of iron(III) hydrolysis in light and heavy water at 25 °C [J]. Journal of

- Inorganic and Nuclear Chemistry, 1975, 37(3): 779-783.
- [41] HUG S J, CANONICA L, WEGELIN M, GECHTER D, von GUNTEN U. Solar oxidation and removal of arsenic at circumneutral pH in iron containing waters [J]. Environmental Science & Technology, 2001, 35(10): 2114–2121.
- [42] WANG K L, JIA Y F. Effects of temperature and pH on the
- transformation of ferric arsenate to scorodite in acidic solution [J]. Advanced Materials Research, 2013, 726-731: 2165-2168.
- [43] WELHAM N J, MALATT K A, VUKCEVIC S. The effect of solution speciation on iron-sulphur-arsenic-chloride systems at 298 K [J]. Hydrometallurgy, 2000, 57(3): 209–223.

砷在酸性溶液体系中的氧化还原行为和化学形态

杨锦琴1, 柴立元1,2, 李青竹1,2, 舒余德1,2

- 1. 中南大学 冶金与环境学院,长沙 410083;
- 2. 中南大学 国家重金属污染防治工程技术研究中心,长沙 410083

摘 要:治炼酸性废水中砷的去除是一项十分紧迫的工作。目前最常用的方法是先将三价砷氧化为五价砷,然后再以铁盐进行沉淀去除。砷的氧化还原行为及化学形态基础研究对于砷的去除意义重大。采用循环伏安法和紫外可见分光光度法开展实验室研究,采用 HSC 和 MINTEQ 软件进行理论分析。研究发现三价砷的氧化是一个多电子转移反应,受扩散控制;在 pH 1.0 的硫酸溶液中,三价砷的氧化过电位非常高(约 0.9 V)。另外,针对 Fe(III)—As(V)—H₂SO₄—H₂O 系列溶液的紫外—可见光谱以及物质形态分析均表明 Fe(III)—As(V)配合物的存在。因此,基于其他研究者预测的热力学数据,绘制 Fe(III)、As(V)的物质形态随 pH 的分布规律图和包含 Fe—As 配合物的新型电位—pH 图。

关键词: 砷; 铁-砷配合物; 电位-pH图; 化学形态; 酸性废水

(Edited by Bing YANG)